Distributed Electric Field Induces Orientations of Nanosheets to Prepare Hydrogels with Elaborate Ordered Structures and Programmed Deformations

Qing Li Zhu, Chen Fei Dai, Daniel Wagner, Matthias Daab, Wei Hong, Josef Breu,* Qiang Zheng, and Zi Liang Wu*

Living organisms use musculatures with spatially distributed anisotropic structures to actuate deformations and locomotion with fascinating functions. Replicating such structural features in artificial materials is of great significance yet remains a big challenge. Here, a facile strategy is reported to fabricate hydrogels with elaborate ordered structures of nanosheets (NSs) oriented under a distributed electric field. Multiple electrodes are distributed with various arrangements in the precursor solution containing NSs and gold nanoparticles. A complex electric field induces sophisticated orientations of the NSs that are permanently inscribed by subsequent photo-polymerization. The resultant anisotropic nanocomposite poly(*N*-isopropylacrylamide) hydrogels exhibit rapid deformation upon heating or photoirradiation, owing to the fast switching of permittivity of the media and electric repulsion between the NSs. The complex alignments of NSs and anisotropic shape change of discrete regions result in programmed deformation of the hydrogels into various configurations. Furthermore, locomotion is realized by a spatiotemporal light stimulation that locally triggers time-variant shape change of the composite hydrogel with complex anisotropic structures. Such a strategy on the basis of the distributed electric-field-generated ordered structures should be applicable to gels, elastomers, and thermosets loaded with other anisotropic particles or liquid crystals, for the design of biomimetic/ bioinspired materials with specific functionalities.

Living organisms use spatiotemporally controlled expansion and contraction of soft tissues with anisotropic structures at different scales to achieve complex 3D deformations, movements, and thereby versatile and fascinating functions.[1] For example,

the mantle of squids mainly comprises two groups of muscle fibers: the circumferential fibers that constitute the bulk of the mantle wall, and the radial fibers that are distributed in the mantle wall as to partition the circumferential ones.[2] Squids expand their mantle radially, filling the mantle cavity with water. Then the circumferential muscles contract, pushing the water out of the mantle cavity through the funnel. Repetition of these movements results in a pulsed jet.

Inspired by these natural systems, there are many efforts devoted to developing soft active materials with anisotropic structures by hybridizing liquid crystals or nanoparticles. Anisotropic materials fulfill specific functions and enable various applications including mass transport,[3] structural colors,[4] actuations,[5,6] and soft robotics.[1a,b,7] In addition, programmable, complex ordered materials display local response under stimuli and show intriguing 3D configurations, imitating actuation or locomotion of living organisms.[6a,e,7c] Although photo- and surface-mediated molecular alignments are versatile to fabricate liquid crystalline elastomer/network films with distributed ordered structures.[6b,8] The thickness and dimensions of the films are usually limited in micrometer scale, and the strategy cannot be extended to other systems like hydrogels with sophisticated alignments. So far, preparation of anisotropic

Q. L. Zhu, C. F. Dai, Prof. Q. Zheng, Prof. Z. L. Wu
Ministry of Education Key Laboratory of Macromolecular, Synthesis and Functionalization
Department of Polymer Science and Engineering
Zhejiang University
Hangzhou 310027, China
E-mail: wuziliang@zju.edu.cn

The ORCID identification number(s) for the author(s) of this article can be found under https://doi.org/10.1002/adma.202005567.

D. Wagner, M. Daab, Prof. J. Breu
Bavarian Polymer Institute and Department of Chemistry
University of Bayreuth
Universitätsstrasse 30, Bayreuth 95440, Germany
E-mail: Josef.Breu@uni-bayreuth.de

Prof. W. Hong
Department of Mechanics and Aerospace Engineering
Southern University of Science and Technology
Shenzhen 518055, China

ADVANCED
SCIENCE NEWS
www.advancedsciencenews.com

ADVANCED
MATERIALS
www.advmat.de

hydrogels mainly relies on molecular self-assembly,[9] mechanical strain/shear,[10] external electric/magnetic fields,[11] and 3D printing[1e,5b,6e] to orient the molecules or nanoparticles before, during, or after the polymerization process. For example, electric or magnetic fields have been used to orient nanoparticles to prepare monodomain hydrogels.[3d,5a,11a] However, it is a major challenge to program the distribution of external fields to form elaborate alignments of nanoparticles in one step. Besides, 3D printing technology is utilized to align nanofillers by mechanical shearing, and the resultant anisotropic hydrogels exhibit biomimetic shape change to form 3D morphologies.[5b] However, this strategy is time-consuming and limited to few specific systems. A facile and general approach is sought after for the design of hydrogels with elaborate ordered structures allowing for programmable deformation and locomotion.

Here, we demonstrate a simple and efficient strategy to fabricate patterned hydrogels with complex ordered structures by generating an intricate yet programmable electric field to induce orientations of highly charged nanosheets (NSs) before the polymerization process. Multiple electrodes are distributed in the precursor solution to complete the intricate orientations in one step, where the NSs align along the electric field.[12] Gold nanoparticles (AuNPs) with high photothermal conversion efficiency are incorporated to afford the anisotropic poly(N-isopropylacrylamide) (PNIPAm) hydrogels with photoresponsibility.[13] The resultant composite hydrogels with intricate ordered structures exhibit fast and isochoric deformations to form various 3D configurations upon heating or light irradiation. Locomotion of the patterned composite hydrogel is realized by using a moving light beam to spatiotemporally trigger the localized deformation. Such a strategy should be applicable to other nanofillers or liquid crystals for the development of soft active materials with biomimetic structures, deformations, and locomotion.

The fluorohectorite $[Na_{0.5}][Li_{0.5}Mg_{2.5}][Si_4]O_{10}F_2$ NSs used in this work have a high aspect ratio of ≈20 000 and a high charge density of 1.1 nm^{-2}. Delamination into single lamellae is achieved by repulsive osmotic swelling in water, producing a nematic phase even at very low content of NS applied here (≈0.3 wt%).[3d,14] As shown in **Figure 1**, the NSs with anisotropic permittivity align along the electric field with a pair of point electrodes, forming a macroscopically ordered spindle-like structure. Before the application of electric field, the nematic suspension of NSs without long-range alignment shows weak birefringence in polarizing optical microscopy (POM). After the high-frequency AC electric field is applied to the suspension for 10 min (Figure S1 and Movie S1, Supporting Information), strong birefringence appears. We should note that the polarity of the electrodes distributed in the precursor solution is frequently and synchronously switched under the application of AC field. According to the birefringence colors, we can identify the localized alignments of the optically positive NSs, which show yellow and blue birefringence colors when oriented in the northwest–southeast and northeast–southwest directions, respectively (Figure S2, Supporting Information). In other words, NSs orient along the electric field to form the spindle-like structure. Such complex ordered structure is well maintained for several minutes after the electric field is switched off, and gradually destroyed over a prolonged period of time due to thermal relaxation (Figure S3, Supporting Information). The electrically oriented structure of NSs can be set permanently by subsequent polymerization of the precursor solution containing N-isopropylacrylamide (NIPAm), chemical crosslinker, and photoinitiator that is completed in 1 min. Systematic experiments are performed to optimize the synthesis parameters for the electrical orientation (Figure S4, Supporting Information). In the following section, we set the electric-field strength of 4 V mm^{-1}, frequency of 10 kHz, and action time of
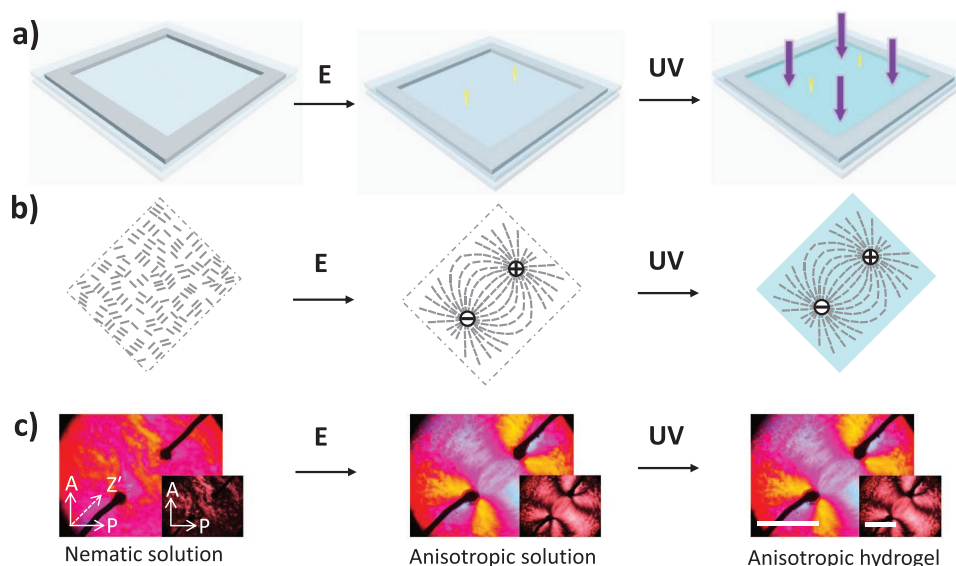
Figure 1. Preparation of hydrogel with intricate ordered structure by a pair of point electrodes with opposite polarities. a) Schematic for the synthesis process of anisotropic hydrogel. b) Schematic for the orientation of NSs induced by the distributed electric field and c) corresponding POM images. Gray rods in (b) represent the NSs; monomer, crosslinker, and photoinitiator are omitted in schematics for simplicity. A: analyzer; P: polarizer; Z′: slow axis of the 530 nm tint plate. Thickness of samples is 2 mm. Scale bars: 5 mm.

2005567 (2 of 8)
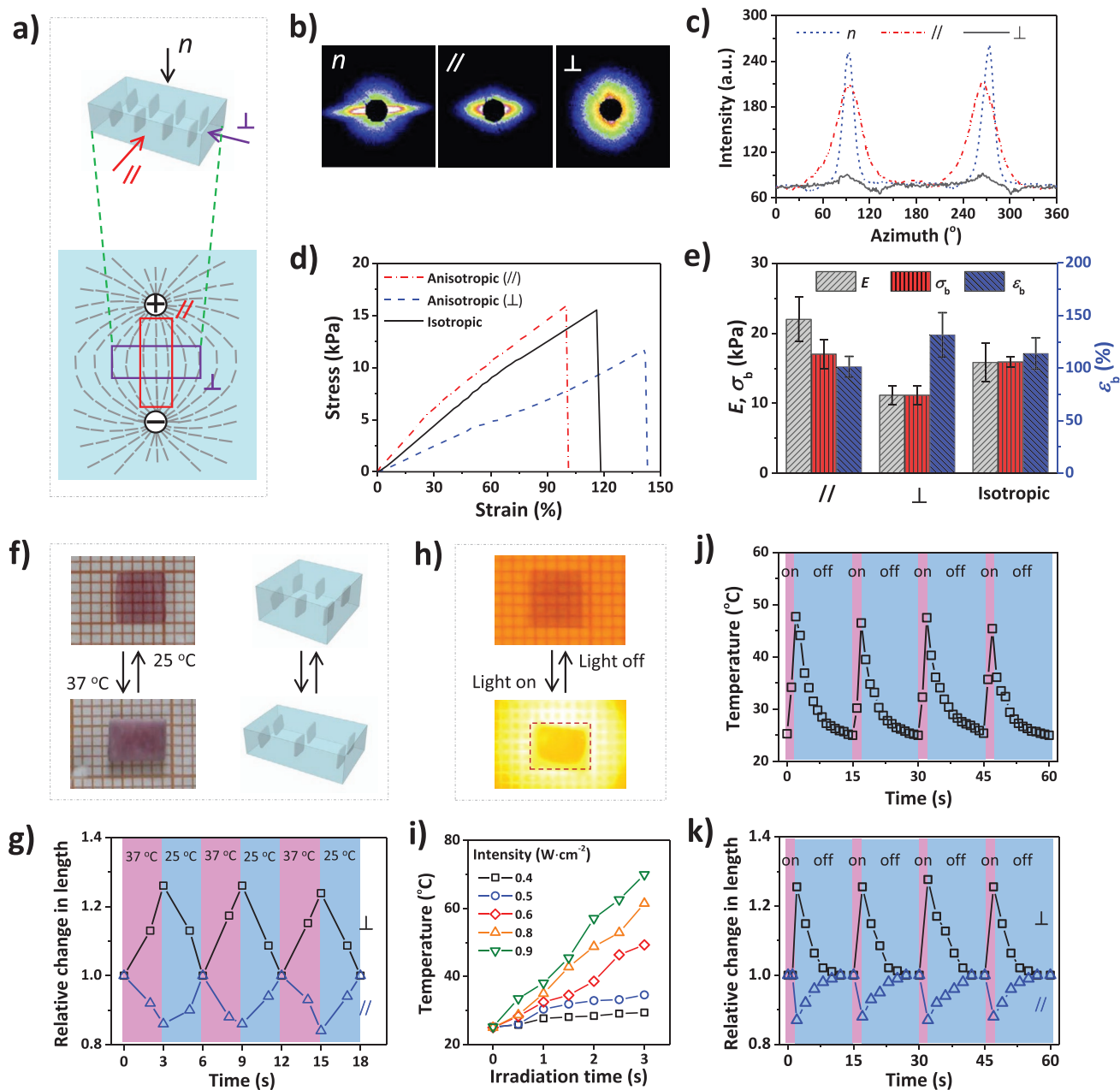
Figure 2. Anisotropic structure, mechanical properties, and responsiveness of the nanocomposite hydrogel. a) Schematic for the alignments of NSs in the composite hydrogel. b) 2D SAXS patterns and c) corresponding azimuthal angle plots of the hydrogel probed from the n, //, and ⊥ directions. d) Tensile strain–stress curves of the gel samples stretched from the // and ⊥ directions and e) corresponding mechanical parameters from three parallel tests. f) Photos, schematic, and g) variations of gel's dimensions upon cyclic incubations in 25 and 37 °C water baths. h) Photos showing the anisotropic shape change of the hydrogel under light irradiation. i) Temperature variations of the hydrogel under irradiation of green light with different power intensity. j) Reversible variations of temperature and k) gel's dimensions under cyclic light irradiation. Light intensity: 0.8 W cm^{-2}; hydrogel thickness: 0.8 mm.

60 min for the electrical orientation of NSs before the synthesis of anisotropic hydrogels.

The anisotropic structure of NSs in the hydrogel (Figure S5, Supporting Information) is further characterized by small-angle X-ray scattering (SAXS). As shown in **Figure 2**a,b, when the X-ray beam is irradiated from the normal (n) and parallel (//) directions, the composite hydrogel exhibits an elliptical diffusive pattern with the longer axis perpendicular

to the direction of electric field. In contrast, isotropic scattering is observed when the X-rays are irradiated from the perpendicular (⊥) direction of the hydrogel. This result confirms that NSs align along the electric field. Accordingly, the azimuth plots of 2D SAXS patterns measured from the n and // directions have two peaks at azimuth angle of 90° and 270° (Figure 2c), corresponding to orientation order parameters of 0.90 and 0.75.

The anisotropic structure affords the hydrogel with anisotropic mechanical properties. Rectangular samples are cut from the central region of the hydrogel along or perpendicular to the connection line of the electrodes (Figure 2a). The hydrogels exhibit a higher Young's modulus (E) in the direction parallel to the alignment of NSs, ≈2 times of that perpendicular to the alignment of NSs (Figure 2d,e). The AuNP-containing hydrogel also shows anisotropic responses to temperature and photo irradiation. After being transferred into hot water (37 °C), the rectangular hydrogel sheet readily undergoes anisotropic, isochoric deformation with expansion perpendicular to the alignment of NSs and contraction parallel to alignment of NSs (Figure 2f). The isochoric deformation of the anisotropic hydrogel is related to the dehydration of PNIPAm chains when the temperature is above the low critical solution temperature (LCST, ≈32 °C). The release of water molecules previously bonded to the polymer chains results in a sudden increase in electrostatic permittivity of the media, leading to an electrostatic repulsion among NSs.[11a] Cyclic immersion of the gel in 25 and 37 °C water bath leads to reversible dimension change (Figure 2g).

The presence of AuNPs endows the hydrogel with a characteristic absorption peak at 520 nm (Figure S6, Supporting Information). Under irradiation with 520 nm green light at intensity of 0.8 W cm^{-2}, the local temperature of the composite hydrogel quickly rises from 25 to 50 °C within 2 s (Figure 2i). Consequently, the hydrogel lengthens by a factor of 1.26 in the direction perpendicular to the alignment of NSs and contracts by a factor of 0.88 in the direction parallel to the alignment of NSs (Figure 2h,k). When the light is switched off, the local temperature returns to 25 °C, accompanied by a recovery of the gel's dimensions to the original ones within 13 s. This photoresponsive behavior is fully reversible (Figure 2j,k; Movie S2, Supporting Information).

The fast anisotropic deformation of hydrogels, especially under the photo irradiation, is beneficial for the programmed deformation and locomotion.[1c,13g] In the following, several hydrogels are designed to demonstrate the control of distributed alignments of NSs by manipulating the electric fields.

As shown in **Figure 3**a, a hydrogel disc with radial alignment of NSs is prepared by using a circular electrode and a point electrode at the center with opposite polarity. Upon heating or light irradiation, the disc gel with radial alignment of NSs buckles into a saddle-shaped configuration, because the gel expands along the azimuthal direction and contracts along the radial direction that results in the built up of compressive hoop stresses. Replacing the circular electrode with a triangular one leads to similar radial alignment of NSs at the central region of the hydrogel (Figure 3b), while the alignments of NSs at the corners are weakened due to the diminishing electric field. This triangular hydrogel also deforms into a saddle-shaped configuration. Simply by varying the shape and arrangement of the electrodes, various composite hydrogels with programmable alignments can be fabricated. As shown in Figure 3c,d, the hydrogels with two or three regions of radial alignments of NSs are obtained, and they deform into sophisticated 3D configurations upon heating or light irradiation.

Hydrogels with periodically ordered structures can also be prepared by using an array of point electrodes to program the distribution of electric field. As aforementioned, NSs orient along the electric field. It is well-known that electric field lines run between the electrodes with opposite polarity rather than those with identical polarity. Therefore, the hydrogel prepared by four electrodes with alternating polarities produces ordered structures similar to concentric alignments (**Figure 4**a). As expected, the gel deforms into a dome-like configuration. In
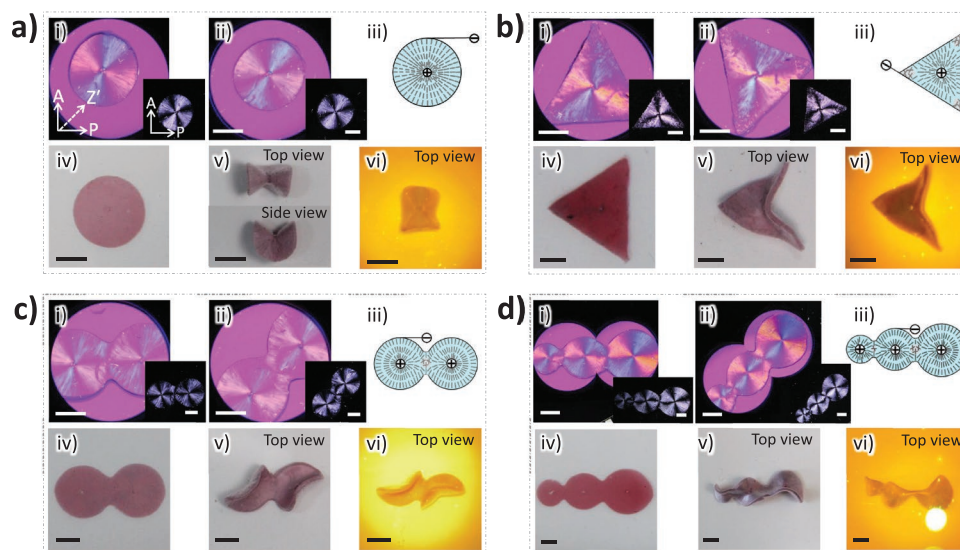
Figure 3. Preparation of hydrogels with radial alignment of NSs and their programmed deformations upon heating or light irradiation. a,b) Hydrogels with radial orientation of NSs prepared by using a circular-shaped (a) or triangular-shaped (b) electrode and a point electrode with opposite polarities and their deformations into saddle-like configurations upon heating or light irradiation. c,d) Hydrogels composed of two (c) or three (d) regions with radial alignments of NSs and their deformations upon heating or light irradiation. In each panel, POM images are taken: i) with and without tint plate and ii) after anticlockwise rotating the sample by 45°. iii) Schematic shows the alignment of NSs and the position of electrodes. iv,v) The photos in the bottom row show the configurations of the hydrogel before (iv) and after (v) the deformation upon heating and vi) upon light irradiation. Thickness of hydrogels is 0.8 mm. Scale bars: 5 mm.
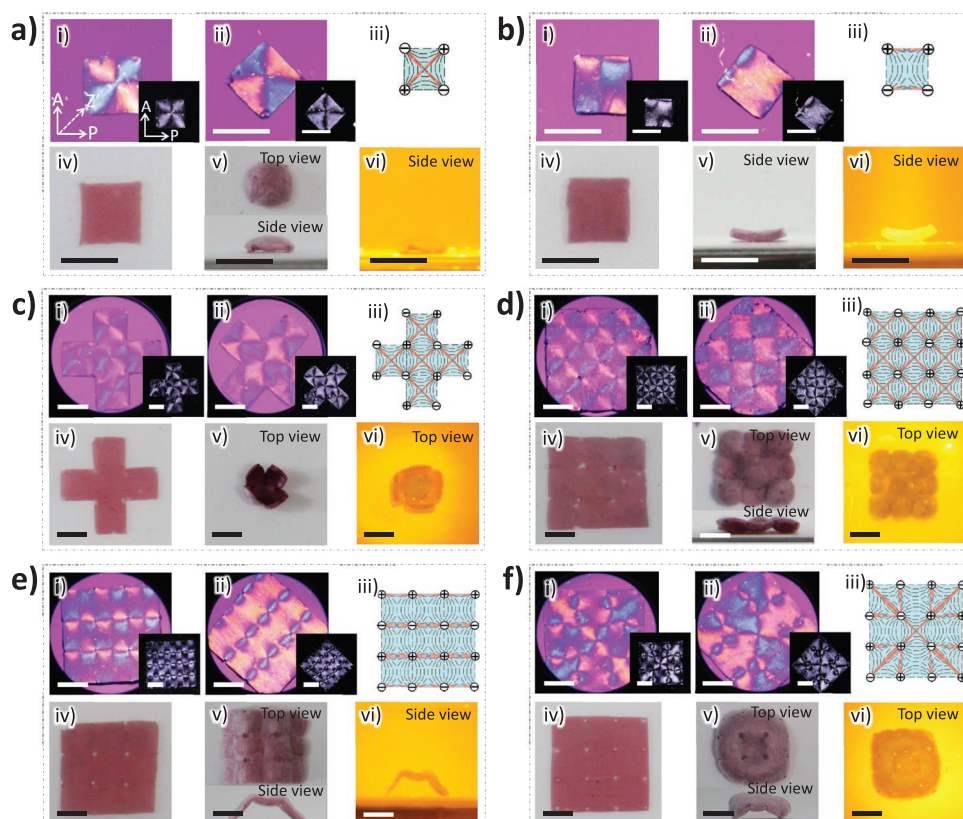
Figure 4. Hydrogels with periodically ordered structures of NSs prepared by distributed electric fields and their programmed deformations upon heating and light irradiation. a) Basic units of hydrogels prepared by four electrodes with alternating polarities and b) parallel-arranged pairs of electrodes with opposite polarities. The gels deform into dome- and arc-shaped configurations, respectively, upon heating or light irradiation. c) Cross-shaped hydrogel with five basic building blocks and its deformation into an open-box configuration. d–f) Patterned hydrogels with nine basic building blocks prepared with the same distribution yet different polarities of point electrodes and their deformations into distinct configurations: d) alternating concave–convex configuration, e) a big rugged arch, and f) a dimpled dome. Thickness of hydrogels is 0.8 mm. Scale bars: 5 mm.

contrast, the hydrogel prepared by two parallel-arranged pairs of electrodes possesses an ordered structure similar to a unidirectional alignment (Figure 4b). Upon heating or light irradiation, the composite hydrogel deforms into an arch configuration since the regions between the two electrodes with the same polarity are isotropic, which constrain the anisotropic deformation of other regions. These two kinds of electrode arrangements and corresponding configurations of hydrogels after stimuli serve as the basic building blocks for patterned hydrogels with periodically ordered structures. As shown in Figure 4c, patterned hydrogels composed of five blocks in the cross-arrangement are facilely prepared by controlling the distribution of electrodes with alternating polarities. Under external stimuli, each unit deforms into a dome configuration, and thus the hydrogel deforms into a configuration resembling an opened box. As the number of blocks further increases, the hydrogel composed of a 3 × 3 array of basic units deforms into a 3D configuration with alternating concave–convex structure (Figure 4d). The neighboring units spontaneously buckle toward opposite directions upon heating or light irradiation. This cooperativity results from the interaction between the neighboring units that buckle upward or downward under stimuli; the buckling of neighboring units in opposite directions can minimize the localized curvature of the connection region and thus the

total elastic energy.[15] By tuning the distributions of electrodes, other patterned hydrogels capable of forming distinct ordered structures can be obtained. As shown in Figure 4e, the hydrogel prepared by parallelly arranged electrodes possesses a quasi-unidirectional alignment of NSs. The isotropic regions between the electrodes of the same polarity constrain the anisotropic deformation of the other regions. Consequently, the gel folds along the connection lines of electrodes with the same polarity and deforms into a rugged arch under external stimuli. When the electrodes are specially arranged as shown in Figure 4f, the overall hydrogel deforms into a dome with the central region buckling downward and forming a concavity. We should note that the shape change of the patterned hydrogels is driven by permittivity-mediated electrostatic repulsion between the NSs, and thus readily completes upon stimuli and is fully reversible, enabling the design of soft robots with fast response.

Two patterned hydrogels are designed to demonstrate the programmed deformation and locomotion under spatiotemporal light irradiation that results in time-variant localized shape change. A ring-shaped hydrogel with radial orientation of NSs is fabricated by using a pair of circular electrodes (**Figure 5**a). When the overall hydrogel is immersed in hot water or irradiated under green light, it deforms into a saddle-like configuration, similar to the disc gel with radial alignment of NSs. When
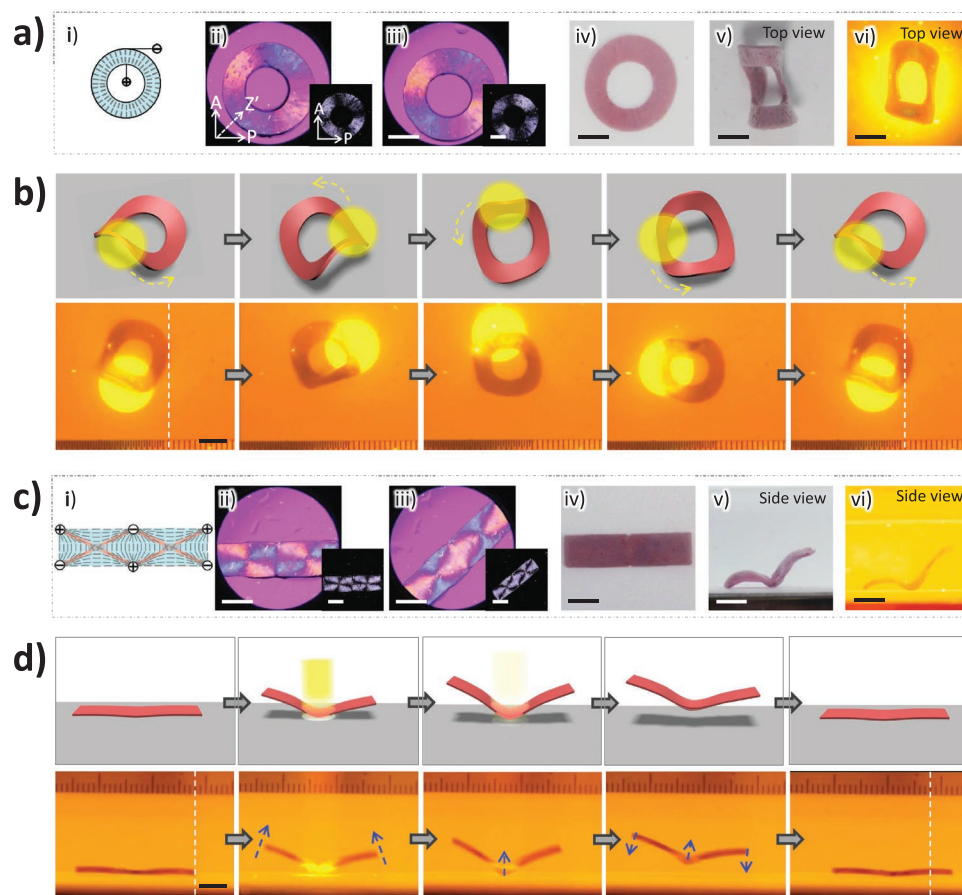
Figure 5. Programmable deformations and locomotion of anisotropic hydrogels under tempospatial light irradiation. a) Preparation of hydrogel ring with radial alignments of NSs and its deformation under heating or light irradiation. b) Snapshots to show the translational and rotary motions of the hydrogel ring under circular scanning of a laser beam with a speed of 1.05 rad s^{-1}. Schematics are presented above the snapshots to show the details. The yellow arrows show the circular scanning direction. c) Preparation of rectangular hydrogel strip with intricately ordered structures and its deformation into 3D configuration upon heating or light irradiation. d) Seagull-like gliding motion of the rectangular hydrogel upon a pulse light irradiation on the central region of the gel strip. The blue arrows represent motion direction of the hydrogel. The white dashed lines indicate the position and displacement of the gel. Laser spot diameter: 11 mm; power intensity: 0.8 W cm^{-2}. Scale bars: 5 mm.

the hydrogel is irradiated by using a laser beam (intensity: 0.8 W cm^{-2}) to scan along the ring shape (speed: 1.05 rad s^{-1}), a traveling buckle is observed, leading to the rocking back and forth and thus rotary and translational motions of the hydrogel (Figure 5b; Movie S3, Supporting Information). The localized irradiation leads to asymmetric deformation and shifts the barycenter of the ring-shaped hydrogel. Repeated light scanning powers and steers the locomotion of the ring-shaped hydrogel.[16]

The second proof-of-concept example is the drifting motion of a patterned hydrogel under localized light stimulation, like the gliding of seagulls. A rectangular hydrogel is prepared following a similar protocol as described above; the ordered structures are confirmed by POM observation and are illustrated in the scheme (Figure 5c). When the integrated hydrogel is heated or irradiated by green light, it deforms into a 3D configuration like a flying seagull. Two discrete regions form dome shapes and are linked by an articulate folding. Locomotion is achieved by localized irradiation (spot diameter: 11 mm; intensity: 0.8 W cm^{-2}) on the fold (Figure 5d; Movie S4, Supporting Information). Owing to the complex ordered structures, the

hydrogel is not flat even when equilibrated in water at room temperature. In the middle region, the NSs orient along the width direction of the rectangular sheet, and the mismatched anisotropic swelling leads to slightly buckling. A short-pulse light irradiation at this region dramatically enhances the buckling downward, and the integrated hydrogel folds upward at a fast speed. After the light irradiation is switched off, the gel is inclined to recover to the original state. Due to the asymmetric hydrodynamic dragging forces, the central region is lifted quickly (≈2 mm within 0.5 s) but settles gradually under gravity (Figure 5d). The sideward drifting by ≈4 mm at settling is due to the geometric asymmetry between the left and the right parts of the composite hydrogel. Such drifting motion is sustainable by repeated light irradiation (Movie S5, Supporting Information). Interestingly, when the hydrogel is turned over with the middle region buckled upward, it quickly bends downward with central part moving upward upon a short-pulse light irradiation, resulting in jump motion of the hydrogel (Movie S6, Supporting Information).

In conclusion, we have developed a facile strategy to prepare hydrogels with elaborate ordered structures by using multiple

electrodes to program the distribution of the electric field that orients the NSs before the polymerization and crosslinking process. These spatially ordered structures afford the hydrogels with controllable deformations and locomotion under external stimuli. Other hydrogels or elastomers with various sophisticated structures can be fabricated by arranging the shape and distribution of electrodes to orient the nanorods/NSs or liquid crystal molecules. These structures can be minimized to micrometer-scale or nanoscale provided the precise control of electrodes; other sophisticated locomotion should be expected by using a structured light for spatiotemporal stimulation.[13g,16b] The resultant programmed deformations and locomotion of the active soft materials, especially those fueled by spatiotemporal light, should find applications as biomedical devices, flexible electronics, soft actuators/robots, and so forth.

Experimental Section

Materials: NIPAm was used as received from Aladdin Chemistry Co., Ltd.; *N,N'*-methylenebis(acrylamide) (MBAA, used as the chemical crosslinker) was purchased from Sigma Aldrich. Lithium phenyl-2,4,6-tri methylbenzoylphosphinate (LAP, used as the photoinitiator) was synthesized according to the protocol reported in the literature.[17] The fluorohectorite NSs of $[Na_{0.5}][Li_{0.5}Mg_{2.5}][Si_4]O_{10}F_2$ were synthesized by melt synthesis at high temperature followed by a long-term annealing process.[14a] AuNPs with the average size of $\approx$10 nm were synthesized according to the reported method.[18] Millipore deionized water was used in all the experiments.

Preparation of Anisotropic Hydrogels: Prescribed amounts of NIPAm (1 M), MBAA (2 mol%, relative to the monomer), and LAP (0.6 mol%, relative to the monomer) were dissolved in water to form a homogeneous aqueous suspension containing 0.27 wt% of NSs and 0.25 wt% of AuNPs (relative to the total mass of the suspension). The precursor solution was injected into a reaction cell consist of a pair of poly(methyl methacrylate) (PMMA) substrates which were separated with 0.8 mm silicon spacer. Holes with diameter of 0.5 mm were distributed in one PMMA substrate to enable the position of Ag electrodes. After applying the AC electric field for 60 min, the NSs were oriented and the reaction cell was immediately exposed to UV light irradiation for 60 s to complete the polymerization and crosslinking reactions. The as-prepared nanocomposite hydrogel was swelled in a large amount of water to remove the residuals and achieve the equilibrium state. Dimensions of the nanocomposite hydrogels with different ordered structures are shown in Figures S7 and S8, Supporting Information.

Characterizations: The birefringence of the precursor solutions during and after the electrical orientation of NSs and the resultant anisotropic hydrogels was observed under a polarizing optical microscope (LV100N POL, Nikon) with and without 530 nm tint plate. To characterize the alignment of NSs, the equilibrated hydrogels were sliced into narrow strips (width: 2 mm) for the observation from different directions. SAXS measurements were conducted on a Xeuss SAXS system (Xenocs SA). X-ray wavelength was 0.154 nm, the beam spot was 172 × 172 μm², and the sample-to-detector distance was 1370 mm. Intensity distribution profile in the azimuthal angle was used to calculate the orientation index (π) according to the equation of $\pi = (180 - H)/180$, where H is the half width of the peak of the azimuthal plot from the selected equatorial reflection.

The mechanical properties of the equilibrated hydrogel were measured by using a tensile tester (Instron 3343). The hydrogels were prepared by using a pair of point electrodes with 10 mm distance, electric-field strength of 4 V mm⁻¹, frequency of 10 kHz, and action time of 60 min. Samples with dimensions of 10 mm × 2 mm × 0.8 mm were cut from the central of the anisotropic hydrogels along or perpendicular to the alignment of NSs. Tensile tests were performed at room temperature

with a gauge length of 5 mm and a stretch rate of 50 mm min⁻¹. Young's modulus was calculated based on the initial slope of the nominal stress–strain curves with a strain below 10%. Young's modulus (E), breaking stress (σ_b), and breaking strain (ε_b) were obtained from three independent samples.

Conflict of Interest

The authors declare no conflict of interest.

[1] a) S. Ma, X. Li, S. Huang, J. Hu, H. Yu, *Angew. Chem., Int. Ed.* **2019**, *58*, 2655; b) M. Wani, H. Zeng, A. Priimagi, *Nat. Commun.* **2017**, *8*, 15546; c) Z. Sun, Y. Yamauchi, F. Araoka, Y. S. Kim, J. Bergueiro, Y. Ishida, Y. Ebina, T. Sasaki, T. Hikima, T. Aida, *Angew. Chem., Int. Ed.* **2018**, *57*, 15772; d) C. Ahn, X. Liang, S. Cai, *Adv. Mater. Technol.* **2019**, *4*, 1900185; e) R. Studart, *Chem. Soc. Rev.* **2016**, *45*, 359.

[2] J. T. Thompson, *J. Exp. Biol.* **2006**, *209*, 433.

[3] a) N. Miyamoto, M. Shintate, S. Ikeda, Y. Hoshida, Y. Yamauchi, R. Motokawa, M. Annaka, *Chem. Commun.* **2013**, *49*, 1082; b) W. Kong, C. Wang, C. Jia, Y. Kuang, G. Pastel, C. Chen, G. Chen, S. He, H. Huang, J. Zhang, S. Wang, L. Hu, *Adv. Mater.* **2018**, *30*, 1801934; c) J. Wu, Q. Zhao, J. Sun, Q. Zhou, *Soft Matter* **2012**, *8*, 362; d) T. Inadomi, S. Ikeda, Y. Okumura, H. Kikuchi, N. Miyamoto, *Macromol. Rapid Commun.* **2014**, *35*, 1741.

[4] a) Y. Zhang, J. Mei, C. Yan, T. Liao, J. Bell, Z. Sun, *Adv. Mater.* **2020**, *32*, 1902806; b) K. Sano, Y. S. Kim, Y. Ishida, Y. Ebina, T. Sasaki, T. Hikima, T. Aida, *Nat. Commun.* **2016**, *7*, 12559; c) R. Kizhakidathazhath, Y. Geng, V. S. R. Jampani, C. Charni, A. Sharma, J. P. F. Lagerwall, *Adv. Funct. Mater.* **2020**, *30*, 1909537.

[5] a) R. M. Erb, J. S. Sander, R. Grisch, A. R. Studart, *Nat. Commun.* **2013**, *4*, 1712; b) S. Gladamn, E. A. Matsumoto, R. G. Nuzzo, L. Mahadevan, J. A. Lewis, *Nat. Mater.* **2016**, *15*, 413.

[6] a) T. J. White, D. J. Broer, *Nat. Mater.* **2015**, *14*, 1087; b) S. Ahn, T. H. Ware, K. M. Lee, V. P. Tondiglia, T. J. White, *Adv. Funct. Mater.* **2016**, *26*, 5819; c) X. Pan, J. Lv, C. Zhu, L. Qin, Y. Yu, *Adv. Mater.*

2019, *31*, 1904224; d) J. Lv, Y. Y. Liu, J. Wei, E. Chen, L. Qin, Y. Yu, *Nature* **2016**, *537*, 179; e) M. Zhang, Y. Wang, M. Jian, C. Wang, X. Liang, J. Niu, Y. Zhang, *Adv. Sci.* **2020**, *7*, 1903048; f) S. Wang, Y. Gao, A. Wei, P. Xiao, Y. Liang, W. Lu, C. Chen, C. Zhang, G. Yang, H. Yao, T. Chen, *Nat. Commun.* **2020**, *11*, 4359; g) F. Ge, Y. Zhao, *Adv. Funct. Mater.* **2020**, *30*, 1901890.

[7] a) B. Zuo, M. Wang, B. Lin, H. Yang, *Nat. Commun.* **2019**, *10*, 4539; b) M. Rogóż, H. Zeng, C. Xuan, D. S. Wiersma, P. Wasylczyk, *Adv. Opt. Mater.* **2016**, *4*, 1689; c) M. Schaffner, J. A. Faber, L. Pianegonda, P. A. Rühs, F. Coulter, A. R. Studart, *Nat. Commun.* **2018**, *9*, 878; d) H. Zeng, P. Wasylczyk, D. S. Wiersma, A. Priimagi, *Adv. Mater.* **2018**, *30*, 1703554.

[8] a) H.-H. Yoon, D.-Y. Kim, K.-U. Jeong, S.-K. Ahn, *Macromolecules* **2018**, *51*, 1141; b) Y. Xia, G. Cedillo-Servin, R. D. Kamien, S. Yang, *Adv. Mater.* **2016**, *28*, 9637; c) H. Aharoni, Y. Xia, X. Zhang, R. D. Kamien, S. Yang, *Proc. Natl. Acad. Sci. U. S. A.* **2018**, *115*, 7206; d) T. H. Ware, M. E. McConney, J. J. Wie, V. P. Tondiglia, T. J. White, *Science* **2015**, *347*, 982; e) T. H. Ware, J. S. Biggins, A. F. Shick, M. Warner, T. J. White, *Nat. Commun.* **2016**, *7*, 10781; f) G. Babakhanova, T. Turiv, Y. Guo, M. Hendrikx, Q.-H. Wei, A. P. H. J. Schenning, D. J. Broer, O. D. Lavrentovich, *Nat. Commun.* **2018**, *9*, 456.

[9] a) K. Kang, J. J. Walish, T. Gorishnyy, E. L. Thomas, *Nat. Mater.* **2007**, *6*, 957; b) R. M. Capito, H. S. Azevedo, Y. S. Velichko, A. Mata, S. I. Stupp, *Science* **2008**, *319*, 1812; c) Z. L. Wu, T. Kurokawa, S. M. Liang, H. Furukawa, J. P. Gong, *J. Am. Chem. Soc.* **2010**, *132*, 10064; d) J. A. Kelly, A. M. Shukaliak, C. C. Y. Cheung, K. E. Shopsowitz, W. Y. Hamad, M. J. MacLachlan, *Angew. Chem., Int. Ed.* **2013**, *52*, 8912; e) L. Qiao, C. Du, J. P. Gong, Z. L. Wu, Q. Zheng, *Adv. Mater. Technol.* **2019**, *4*, 1900665.

[10] a) M. A. Haque, G. Kamita, T. Kurokawa, K. Tsujii, J. P. Gong, *Adv. Mater.* **2010**, *22*, 5110; b) S. M. Zhang, M. A. Greenfield, A. Mata, L. C. Palmer, R. Bitton, J. R. Mantei, C. Aparicio, M. O. de la Cruz, S. I. Stupp, *Nat. Mater.* **2010**, *9*, 594; c) R. Takahashi, Z. L. Wu, M. Arifuzzaman, T. Nonoyama, T. Nakajima, T. Kurokawa, J. P. Gong, *Nat. Commun.* **2014**, *5*, 4490; d) C. Zhao, P. Zhang, J. Zhou, S. Qi, Y. Yamauchi, R. Shi, R. Fang, Y. Ishida, S. Wang, A. P. Tomsia, M. Liu, L. Jiang, *Nature* **2020**, *580*, 210.

[11] a) Y. S. Kim, M. Liu, Y. Ishida, Y. Ebina, M. Osada, T. Sasaki, T. Hikima, M. Takata, T. Aida, *Nat. Mater.* **2015**, *14*, 1002;

b) L. Wu, M. Ohtani, M. Takata, A. Saeki, S. Seki, Y. Ishida, T. Aida, *ACS Nano* **2014**, *8*, 4640; c) S. Yook, S. S. Eshaghi, A. Yildirim, Z. Mutlu, M. Cakmak, *Soft Matter* **2019**, *15*, 9733; d) Y. Wang, Y. Chen, J. Gao, H. G. Yoon, L. Jin, M. Forsyth, T. J. Dingemans, L. A. Madsen, *Adv. Mater.* **2016**, *28*, 2571.

[12] a) I. Dozov, E. Paineau, P. Davidson, K. Antonova, C. Baravian, I. Bihannic, L. J. Michot, *J. Phys. Chem. B* **2011**, *115*, 7751; b) E. Paineau, A. Philippe, K. Antonova, I. Bihannic, P. Davidson, I. Dozov, J. P. Gabriel, M. Impérorclerc, P. Levitz, F. Meneau, L. J. Michot, *Liq. Cryst. Rev.* **2013**, *1*, 110.

[13] a) A. Suzuki, T. Tanaka, *Nature* **1990**, *346*, 345; b) S. R. Sershen, G. A. Mensing, M. Ng, N. J. Halas, D. J. Beebe, J. L. West, *Adv. Mater.* **2005**, *17*, 1366; c) D. Kim, H. S. Lee, J. Yoon, *RSC Adv.* **2014**, *4*, 25379; d) E. Wang, M. S. Desai, S.-W. Lee, *Nano Lett.* **2013**, *13*, 2826; e) J. Yoon, P. Bian, J. Kim, T. J. McCarthy, R. C. Hayward, *Angew. Chem., Int. Ed.* **2012**, *51*, 7146; f) A. Barhoumi, W. Wang, D. Zurakowski, R. S. Langer, D. S. Kohane, *Nano Lett.* **2014**, *14*, 3697; g) A. W. Hauser, A. A. Evans, J.-H. Na, R. C. Hayward, *Angew. Chem. Int. Ed.* **2015**, *127*, 5524; h) H. Kim, J.-H. Kang, Y. Zhou, A. S. Kuenstler, Y. Kim, C. Chen, T. Emrick, R. C. Hayward, *Adv. Mater.* **2019**, *31*, 1900932.

[14] a) S. Rosenfeldt, M. Stöter, M. Schlenk, T. Martin, R. Q. Albuquerque, S. Förster, J. Breu, *Langmuir* **2016**, *32*, 10582; b) M. Stöter, D. A. Kunz, M. Schmidt, D. Hirsemann, H. Kalo, B. Putz, J. Senker, J. Breu, *Langmuir* **2013**, *29*, 1280; c) M. Daab, S. Rosenfeldt, H. Kalo, M. Stöter, B. Bojer, R. Siegel, S. Förster, J. Senker, J. Breu, *Langmuir* **2017**, *33*, 4816.

[15] a) Z. J. Wang, C. N. Zhu, W. Hong, Z. L. Wu, Q. Zheng, *Sci. Adv.* **2017**, *3*, e1700348; b) P. Ma, B. Niu, J. Lin, T. Kang, J. Qian, Z. L. Wu, Q. Zheng, *Macromol. Rapid Commun.* **2019**, *40*, 1800681; c) X. P. Hao, Z. Xu, C. Y. Li, W. Hong, Q. Zheng, Z. L. Wu, *Adv. Mater.* **2020**, *32*, 2000781.

[16] a) Z. Song, L. Ren, C. Zhao, H. Liu, Z. Yu, Q. Liu, L. Ren, *ACS Appl. Mater. Interfaces* **2020**, *12*, 6351; b) S. Palagi, A. G. Mark, S. Y. Reigh, K. Melde, T. Qiu, H. Zeng, C. Parmeggiani, D. Martella, A. Sanchez-Castillo, N. Kapernaum, F. Giesselmann, D. S. Wiersma, E. Lauga, P. Fischer, *Nat. Mater.* **2016**, *15*, 647.

[17] T. Majima, W. Schnabel, W. Weber, *Makromol. Chem.* **1991**, *192*, 2307.

[18] G. Frens, Z. Kolloid, *Nat. Phys. Sci.* **1973**, *241*, 20.